Commun. Comput. Phys.
doi: 10.4208/cicp.scpde14.32s

Vol. **19**, No. 5, pp. 1375-1396
May 2016

Novel Symplectic Discrete Singular Convolution Method for Hamiltonian PDEs

Wenjun Cai[1,2], Huai Zhang[1] and Yushun Wang[2,*]

[1] *Key Laboratory of Computational Geodynamics, University of Chinese Academy of Sciences, Beijing 100049, China.*
[2] *Jiangsu Provincial Key Laboratory for NSLSCS, School of Mathematical Sciences, Nanjing Normal University, Nanjing 210023, China.*

Received 28 February 2015; Accepted (in revised version) 29 December 2015

Abstract. This paper explores the discrete singular convolution method for Hamiltonian PDEs. The differential matrices corresponding to two delta type kernels of the discrete singular convolution are presented analytically, which have the properties of high-order accuracy, bandlimited structure and thus can be excellent candidates for the spatial discretizations for Hamiltonian PDEs. Taking the nonlinear Schrödinger equation and the coupled Schrödinger equations for example, we construct two symplectic integrators combining this kind of differential matrices and appropriate symplectic time integrations, which both have been proved to satisfy the square conservation laws. Comprehensive numerical experiments including comparisons with the central finite difference method, the Fourier pseudospectral method, the wavelet collocation method are given to show the advantages of the new type of symplectic integrators.

AMS subject classifications: 35Q55, 37K05, 65P10, 65M20, 65M70

Key words: Discrete singular convolution, differential matrix, symplectic integrator, Hamiltonian PDEs.

1 Introduction

Non-dissipative phenomena in quantum physics, fluid mechanics, oceanography, electromagnet field and other sciences are often modeled by the Hamiltonian systems of ordinary differential equations (ODEs) and partial differential equations (PDEs). Symplectic integrator is usually attached to a numerical scheme that intends to solve such a Hamiltonian system approximately, while preserving one or more intrinsic properties of the original system, such as the symplectic structure. There are various symplectic

*Corresponding author. *Email addresses:* wenjuncai1@gmail.com (W. Cai), hzhang@ucas.ac.cn (H. Zhang), wangyushun@njnu.edu.cn (Y. Wang)

 ©2016 Global-Science Press

https://doi.org/10.4208/cicp.scpde14.32s Published online by Cambridge University Press

schemes for Hamiltonian ODEs, one can refer to [1–4] for details. The most obvious generalization of the concept of a symplectic integrator to Hamiltonian PDEs is a numerical scheme which is designed to preserve a semi-discretization of the symplectic form associated with the infinite-dimensional evolution equation. The crucial part is how to guarantee the semi-discretization in a finite-dimensional Hamiltonian system. A general approach is that, instead of discretizing the PDE directly, we discretize both the Hamiltonian functional and the Hamiltonian (Poisson) structure, then form the resulting ODEs. The Hamiltonian functional can be discretized in any suitable way, being careful to maintain the symmetry of any derivatives in the functional. For the Hamiltonian structure, replacing the differential operators with any appropriate matrix difference operator may discretize it. The conventional semi-discrete methods are based on the finite difference method (FDM) [5, 6], the Fourier pseudospectral method (PSM) [7, 8], the wavelet collocation method (WCM) [9–11] and they have been applied on sorts of applications like the nonlinear wave equation [12], the Schrödinger equation [13, 14], the Maxwell's equations [15, 16], the KdV equation [5], the Gross-Pitaevskii equation [17, 18] and so on. Numerical experiments show that the corresponding symplectic schemes are superior to other non-symplectic schemes.

This paper presents a new type of semi-discrete method which is the discrete singular convolution method. Such method can be constructed to preserve the symplecticity of the semi-discrete system. The discrete singular convolution (DSC) method was first proposed in [19, 20] for the Fokker-Planck equation and then widely applied on many other partial differential equations including the Fisher's equation [21], the heat equation, the wave equation, the Navier-Stokes equation [22], the sine-Gordon equation [23] and the KdV equation [24]. The first combination of the DSC method and the symplectic method is given by Li [25] for the elastic wave modeling in order to deal with the seismic wave propagation. In this paper, we give the analytical expression of the differential matrices corresponding to the DSC method and apply the DSC method to systematically construct symplectic integrators for general Hamiltonian PDEs.

Comparing with the FDM, PSM, WCM, the DSC algorithm has the following advantages:

1 The DSC method is a generalization of the standard FDM because one can adjust the free parameters in the DSC method to get the central difference scheme (i.e. $\frac{1}{2h}$, 0, $-\frac{1}{2h}$) for the first order derivative and $\frac{1}{h^2}$, $-\frac{2}{h^2}$, $\frac{1}{h^2}$ for the second order derivative where h is the spatial grid step. However, the DSC method is usually much more accurate than the FDM.

2 Such method is as accurate as the PSM for the bandlimited periodic functions and can be even more accurate than the PSM for approximating non-bandlimited functions [22]. Since the DSC method is a local approach, it is more flexible than the PSM in dealing with complex geometry and boundary conditions.

3 The differential matrices for the DSC method can be given explicitly while a recurrence algorithm has to be imposed for deriving the differential matrices for the

https://doi.org/10.4208/cicp.scpde14.32s Published online by Cambridge University Press

WCM. Furthermore, there is no restriction on the computational interval for the DSC method while the WCM needs the endpoints to be integers, otherwise a coordinate transformation must be requested. The partition of the DSC method can be arbitrary while the WCM must be located at dyadic points.

The rest of this paper is organized as follows. In Section 2, we present analytical expressions of the differential matrices for the DSC method with two type of delta kernels respectively and discuss several properties of them. In Section 3, we construct symplectic schemes for the nonlinear Schrödinger equation and coupled Schrödinger equations based on DSC differential matrices. In Section 4, comprehensive numerical experiments including comparisons with the FDM, PSM and WCM are given. Finally, we draw some conclusions in Section 5.

2 Discrete singular convolution differential matrix

In this section, we briefly review the discrete singular convolution approximation for solving partial differential equations [19–21]. Based on the regularized Shannon's kernel and Dirichlet kernel, we give the analytical expressions of the corresponding differential matrices and some discussions on their properties.

Let $\{x_j\}, j=1,2,\cdots,N+1$ be a set of uniform grid points with step h of the computational domain $[a,b]$, $x_1=a$, $x_{N+1}=b$. $\{u_j\}$ is the set of corresponding function values. In the DSC algorithm, we approximate the function u and its kth order derivatives at point x_i by a discrete convolution

$$\frac{\partial^k u}{\partial x^k}\Big|_{x=x_i} \approx \sum_{j=i-M}^{i+M} \delta^{(k)}_{\alpha,\sigma}(x_i-x_j)u_j, \quad (k=0,1,2,\cdots), \tag{2.1}$$

where $2M+1$ is the computational bandwidth. Here $\delta_{\alpha,\sigma}$ is a collective symbol for one of the (regularized) DSC kernels, or in general, any delta sequence kernel providing an approximation to the delta distribution δ. For a given $\delta_{\alpha,\sigma}(x-x_j)$, the higher order derivatives can be obtained directly by the analytical differentiation. Delta sequence kernels can be constructed as either positive type or Dirichlet type. Here we only consider two kernels of Dirichlet type, i.e., the regularized Shannon's kernel (RSK) and the regularized Dirichlet kernel (RDK)

$$\delta_{\pi/h,\sigma}(x-x_j)=\frac{\sin\left[\frac{\pi}{h}(x-x_j)\right]}{\frac{\pi}{h}(x-x_j)}\exp\left[-\frac{(x-x_j)^2}{2\sigma^2}\right], \tag{2.2}$$

$$\delta_{\pi/h,\sigma}(x-x_j)=\frac{\sin\left[\frac{\pi}{h}(x-x_j)\right]}{L\sin\left[\frac{\pi}{h}\frac{x-x_j}{L}\right]}\exp\left[-\frac{(x-x_j)^2}{2\sigma^2}\right], \tag{2.3}$$

where σ is a parameter for optimizing the numerical result and is always proportion to the grid step $r=\sigma/h$. L is an odd integer which also can be optimized to achieve better

https://doi.org/10.4208/cicp.scpde14.32s Published online by Cambridge University Press

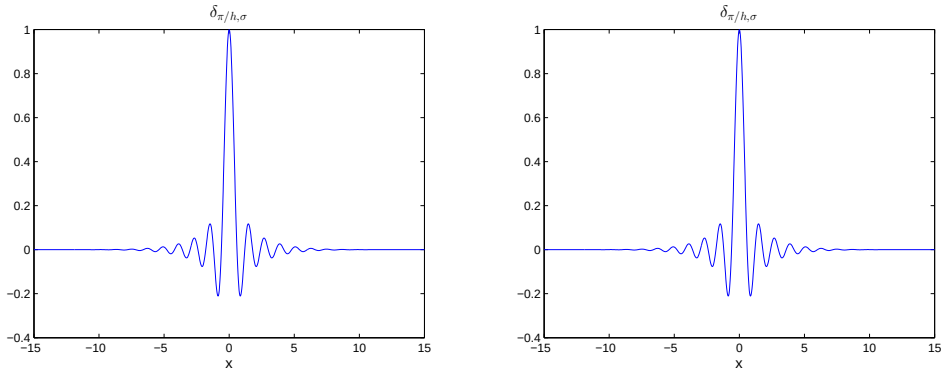


Figure 1: The base functions of RSK (left) and RDK (right).

result. The RSK and RDK are sets of local base functions. Fig. 1 plots profiles of the RSK and RDK base functions with grid step $h=0.6$, $\sigma=3.5$, $L=71$. It is noticed that both base functions are compactly supported with almost the same shape. As $L\to\infty$, the RDK converts to the RSK.

A mathematical estimation for the choice of M,σ and h is given in [20]. For example, if the L^2 error for approximating an L^2 function f is set to $10^{-\eta}$ $(\eta>0)$, the following relations have to be satisfied

$$r(\pi-Bh)>\sqrt{4.61\eta}, \quad \text{and} \quad \frac{M}{r}>\sqrt{4.61\eta}, \tag{2.4}$$

where B is the frequency bound for the function f. The first inequality states that for a given grid size h, a large r is requested for approximating an L^2 function with high frequency. The second inequality indicates that if one choose $r=3$, then the half bandwidth $M\sim 30$ can be taken to ensure the highest accuracy in a double precision computation $(\eta=15)$.

We can analytically calculate the derivatives of these two kernels at the grid points x_i, $i=1,2,\cdots,N,N+1$. Here we only present the expressions of first three derivatives, the rest can also be easily obtained. For the RSK, we have

$$\delta^{(1)}_{\pi/h,\sigma}(x_i-x_j)=\begin{cases}\dfrac{(-1)^{i-j}}{h(i-j)}\exp\Big[-\dfrac{(i-j)^2}{2r^2}\Big], & i\neq j,\\ 0, & i=j,\end{cases} \tag{2.5}$$

$$\delta^{(2)}_{\pi/h,\sigma}(x_i-x_j)=\begin{cases}\dfrac{(-1)^{i-j+1}\cdot\lambda_2^S}{h^2(i-j)^2}\exp\Big[-\dfrac{(i-j)^2}{2r^2}\Big], & i\neq j,\\ -\dfrac{\pi^2r^2+3}{3h^2r^2}, & i=j,\end{cases} \tag{2.6}$$

https://doi.org/10.4208/cicp.scpde14.32s Published online by Cambridge University Press

$$\delta^{(3)}_{\pi/h,\sigma}(x_i-x_j)=\begin{cases}\dfrac{(-1)^{i-j}\cdot\lambda_3^S}{h^3(i-j)^3}\exp\Big[-\dfrac{(i-j)^2}{2r^2}\Big], & i\neq j,\\ 0, & i=j,\end{cases} \tag{2.7}$$

where

$$\lambda_2^S=2(r^2+(i-j)^2)/r^2,$$
$$\lambda_3^S=(3(i-j)^4+(3r^2-\pi^2r^4)(i-j)^2+6r^4)/r^4.$$

For the RDK, let $\mu=\pi(i-j)/L$, the derivatives are

$$\delta^{(1)}_{\pi/h,\sigma}(x_i-x_j)=\begin{cases}\dfrac{(-1)^{i-j}\pi\csc(\mu)}{hL}\exp\Big[-\dfrac{(i-j)^2}{2r^2}\Big], & i\neq j,\\ 0, & i=j.\end{cases} \tag{2.8}$$

$$\delta^{(2)}_{\pi/h,\sigma}(x_i-x_j)=\begin{cases}\dfrac{(-1)^{i-j+1}\pi\csc(\mu)\cdot\lambda_2^D}{h^2L^2}\exp\Big[-\dfrac{(i-j)^2}{2r^2}\Big], & i\neq j,\\ \dfrac{\pi^2}{3h^2L^2}-\dfrac{\pi^2r^2+3}{3h^2r^2}, & i=j,\end{cases} \tag{2.9}$$

$$\delta^{(3)}_{\pi/h,\sigma}(x_i-x_j)=\begin{cases}\dfrac{(-1)^{i-j}\pi\csc(\mu)\cdot\lambda_3^D}{h^3L^3}\exp\Big[-\dfrac{(i-j)^2}{2r^2}\Big], & i\neq j,\\ 0, & i=j,\end{cases} \tag{2.10}$$

where

$$\lambda_2^D=\big[2\pi r^2\cot(\mu)+2L(i-j)\big]/r^2,$$
$$\lambda_3^D=\Big[\big(3(i-j)^2-3r^2-\pi^2r^4\big)L^2+6(i-j)\pi r^2L\cot(\mu)$$
$$+3\pi^2r^4\big(\cot^2(\mu)+\csc^2(\mu)\big)\Big]/r^4.$$

Consider $u(x)$ as a periodic function and denote D_k the corresponding kth differential matrices of u, $k=1,2,\cdots$. For convenience, let $d^{(k)}(l):=\delta^{(k)}_{\pi/h,\sigma}(x_i-x_j)$, $l=i-j$. Here, the delta kernel can be chosen as either RSK or RDK. Note that, from (2.1), j is bandlimited for each i. Thus, l is arranged from $-M$ to M. Then we can explicitly give the matrices D_k

$$(D_k)_{i,j}=\begin{cases}d^{(k)}(i-j), & -M\le j-i\le M,\\ d^{(k)}(-s), & i-j=N-s,\ 1\le s\le M,\\ d^{(k)}(s), & j-i=N-s,\ 1\le s\le M,\\ 0, & \text{otherwise.}\end{cases} \tag{2.11}$$

Due to the expressions of $\delta^{(k)}_{\pi/h,\sigma}(x_i-x_j)$, we have the following properties for the differential matrices D_k

https://doi.org/10.4208/cicp.scpde14.32s Published online by Cambridge University Press

(i) D_{2k} is symmetric while D_{2k+1} is skew-symmetric.

(ii) D_k is a circulant matrix with bandwidth of $2M+1$.

(iii) For the calculation of the product D_kU, where $U=(u_1,u_2,\cdots,u_N)^T$, one can use the fast Fourier transform (FFT) to make it much faster. Note that the first column of D_k is

$$\boldsymbol{c}=\left(d^{(k)}(0),d^{(k)}(1)\cdots,d^{(k)}(M),\mathbf{0},d^{(k)}(-M),\cdots,d^{(k)}(-2),d^{(k)}(-1)\right)^T. \tag{2.12}$$

Therefore, let $d^{(k)}=fft(\boldsymbol{c})$, then

$$D_kU=ifft\left(d^{(k)}\cdot fft(U)\right), \tag{2.13}$$

where *fft* and *ifft* are the functions of discrete Fourier transform and inverse discrete Fourier transform in MATLAB. The product in the bracket represents the element-wise product.

3 Two sample symplectic schemes based on the DSC discretization

In this section, we present two symplectic schemes based on the DSC differential matrices (2.11) for the nonlinear Schrödinger (NLS) equation and coupled Schrödinger (CNLS) equations respectively. The NLS equation is an example of a universal nonlinear model that describes many physical nonlinear systems. It has frequently been taken as the test bed to evaluate the behaviors of numerical methods including the symplectic schemes, for example [8, 11, 12]. The coupled structure makes the CNLS equations another ideal test sample for the symplectic integrators as well other numerical methods. Therefore, we choose these two equations to check the numerical performance of the DSC method.

Consider the following NLS equation

$$\mathrm{i}u_t+u_{xx}+\varepsilon|u|^2u=0,\quad x\in[a,b], \tag{3.1}$$

with periodic boundary condition and initial condition

$$u(x,0)=u_0(x), \tag{3.2}$$

where $\mathrm{i}=\sqrt{-1}$ and ε is a real parameter. Let $u(x,t)=p(x,t)+\mathrm{i}q(x,t)$, the NLS equation (3.1) can be written as

$$\begin{aligned} &p_t+q_{xx}+\varepsilon(p^2+q^2)q=0,\\ &q_t-p_{xx}-\varepsilon(p^2+q^2)p=0, \end{aligned} \tag{3.3}$$

which can be further formed into a Hamiltonian system

$$\frac{d}{dt}\boldsymbol{z}=J^{-1}\frac{\delta\mathcal{H}}{\delta\boldsymbol{z}}, \tag{3.4}$$

https://doi.org/10.4208/cicp.scpde14.32s Published online by Cambridge University Press

where $\boldsymbol{z}=(p,q)^T$, $J=\begin{pmatrix} 0 & 1 \\ -1 & 0 \end{pmatrix}$, and

$$\mathcal{H}(\boldsymbol{z})=\int_a^b \frac{1}{2}\Big[\frac{1}{2}\varepsilon(p^2+q^2)^2-p_x^2-q_x^2\Big]dx. \tag{3.5}$$

In order to derive the symplectic scheme, we have to discretize the Hamiltonian (3.5) which is taken as

$$H=\frac{1}{2}\Big[\frac{1}{2}\varepsilon\big\langle(P^2+Q^2)^2,\mathbf{1}\big\rangle+\langle P,D_2P\rangle+\langle Q,D_2Q\rangle\Big], \tag{3.6}$$

where $P=(p_1,p_2,\cdots,p_N)^T$, $Q=(q_1,q_2,\cdots,q_N)^T$ and $P^2=p_jp_j$. Here we adopt Einstein summation convention. $\langle\cdot,\cdot\rangle$ is the standard inner product. Let $Z=(P^T,Q^T)^T$, then we obtain a discrete Hamiltonian system

$$\frac{d}{dt}Z=\begin{pmatrix} 0 & -I \\ I & 0 \end{pmatrix}\begin{pmatrix} \nabla_P H(P,Q) \\ \nabla_Q H(P,Q) \end{pmatrix}. \tag{3.7}$$

Applying the implicit midpoint method on the time integration, we have the following symplectic DSC scheme for the NLS equation (3.1)

$$\begin{aligned} &\frac{P^{n+1}-P^n}{\tau}+D_2Q^{n+\frac{1}{2}}+\varepsilon\Big((P^{n+\frac{1}{2}})^2+(Q^{n+\frac{1}{2}})^2\Big)Q^{n+\frac{1}{2}}=0,\\ &\frac{Q^{n+1}-Q^n}{\tau}-D_2P^{n+\frac{1}{2}}-\varepsilon\Big((P^{n+\frac{1}{2}})^2+(Q^{n+\frac{1}{2}})^2\Big)P^{n+\frac{1}{2}}=0, \end{aligned} \tag{3.8}$$

where $P^{n+\frac{1}{2}}=(P^{n+1}+P^n)/2$, $Q^{n+\frac{1}{2}}=(Q^{n+1}+Q^n)/2$. In the complex form $U=P+\mathrm{i}Q$, the scheme becomes

$$\mathrm{i}\frac{U^{n+1}-U^n}{\tau}+D_2U^{n+\frac{1}{2}}+\varepsilon|U^{n+\frac{1}{2}}|^2U^{n+\frac{1}{2}}=0. \tag{3.9}$$

Define the discrete inner product and the L^2 norm

$$\langle U,V\rangle=h\sum_{j=1}^{N}U_j\bar{V}_j,\quad \|U\|=\langle U,U\rangle^{\frac{1}{2}},$$

we will give the L^2 stability of the scheme (3.8) and its equivalent scheme (3.9).

Proposition 3.1. The scheme (3.8) or (3.9) is unconditionally stable in the L^2 norm.

Proof. Taking the discrete inner product on the two equations of (3.8) with $Q^{n+\frac{1}{2}}$ and $P^{n+\frac{1}{2}}$ respectively, and adding the results together yield

$$\frac{1}{\tau}(\|P^{n+1}\|^2+\|Q^{n+1}\|^2-\|P^n\|^2-\|Q^n\|^2)+\Big\langle P^{n+\frac{1}{2}},D_2Q^{n+\frac{1}{2}}\Big\rangle-\Big\langle Q^{n+\frac{1}{2}},D_2P^{n+\frac{1}{2}}\Big\rangle=0.$$

https://doi.org/10.4208/cicp.scpde14.32s Published online by Cambridge University Press

Due to the symmetry of the differential matrix D_2, the last two terms vanish and we have

$$\|P^{n+1}\|^2+\|Q^{n+1}\|^2=\|P^n\|^2+\|Q^n\|^2,$$

which is equivalent to

$$\|U^{n+1}\|^2=\|U^n\|^2.$$

The proof is complete. □

Remark 3.1. Note that the scheme (3.8) or (3.9) is nothing different from the reported schemes in [8] and [11] expect the expression of the second order differential matrix D_2. One can replace it with the corresponding differential matrices generated by the FDM, PSM and WCM which also lead to symplectic schemes with unconditional stability. In the numerical simulation especially for long-time problems, such conservative property plays a rather important role to guarantee the numerical stability which cannot be achieved with only the improvement of accuracy. Therefore, our proposed symplectic scheme is expected to have superior behaviours in the following numerical experiments.

Remark 3.2. It should also be noticed that there are many higher order symplectic Runge-Kutta methods in the literature (please refer to [3]), we only adopt the second order midpoint scheme here due to the above conservative property and the simplicity for illustration. Recently, the discontinuous Galerkin method is taken into the construction of symplectic methods [26] which combines the condition for the weighted function and the original symplectic conditions [3]. Besides the conventional symplectic methods, some new symplectic Runge-Kutta methods have also been proposed through such methodology. Further comparisons of these methods are worth to be carried both in the theoretical and numerical aspects.

For the following CNLS equations

$$\begin{aligned} &\mathrm{i}u_t+\kappa u_{xx}+(|u|^2+\beta|v|^2)u=0,\\ &\mathrm{i}v_t+\kappa v_{xx}+(|v|^2+\beta|u|^2)v=0, \quad x\in[a,b], \end{aligned} \tag{3.10}$$

with the initial conditions

$$u(x,0)=u_0(x), \quad v(x,0)=v_0(x), \tag{3.11}$$

and zero boundary conditions

$$u(a,t)=u(b,t)=0. \tag{3.12}$$

The related Hamiltonian system is

$$\frac{d}{dt}z=\begin{pmatrix} 0 & 0 & -1 & 0\\ 0 & 0 & 0 & -1\\ 1 & 0 & 0 & 0\\ 0 & 1 & 0 & 0 \end{pmatrix}\frac{\delta\widehat{\mathcal{H}}}{\delta z}, \tag{3.13}$$

https://doi.org/10.4208/cicp.scpde14.32s Published online by Cambridge University Press

where $z=(p,\hat{p},q,\hat{q})^T$, $u=p+\mathrm{i}q$, $v=\hat{p}+\mathrm{i}\hat{q}$ and the Hamiltonian

$$\widehat{\mathcal{H}}(z)=\int_a^b \frac{1}{2}\Big[\frac{1}{2}(p^2+q^2)^2+\frac{1}{2}(\hat{p}^2+\hat{q}^2)^2-\kappa(p_x^2+q_x^2+\hat{p}_x^2+\hat{q}_x^2)+\beta(p^2+q^2)(\hat{p}^2+\hat{q}^2)\Big]dx. \quad (3.14)$$

We can apply the similar procedure as that for the NLS equation to derive the symplectic DSC scheme for the CNLS equation (3.10)

$$\begin{aligned}
&\mathrm{i}\frac{U^{n+1}-U^n}{\tau}+\kappa D_2 U^{n+\frac{1}{2}}+\Big(|U^{n+\frac{1}{2}}|^2+\beta|V^{n+\frac{1}{2}}|^2\Big)U^{n+\frac{1}{2}}=0,\\
&\mathrm{i}\frac{V^{n+1}-V^n}{\tau}+\kappa D_2 V^{n+\frac{1}{2}}+\Big(|V^{n+\frac{1}{2}}|^2+\beta|U^{n+\frac{1}{2}}|^2\Big)V^{n+\frac{1}{2}}=0,
\end{aligned} \quad (3.15)$$

with the corresponding discrete Hamiltonian

$$\begin{aligned}
\widehat{H}=\frac{1}{2}\Big[&\frac{1}{2}\big\langle(P^2+Q^2)^2+(\widehat{P}^2+\widehat{Q}^2)^2,\mathbf{1}\big\rangle+\big\langle\beta(P^2+Q^2)(\widehat{P}^2+\widehat{Q}^2),\mathbf{1}\big\rangle\\
&+\kappa\big(\langle P,D_2P\rangle+\langle Q,D_2Q\rangle+\langle\widehat{P},D_2\widehat{P}\rangle+\langle\widehat{Q},D_2\widehat{Q}\rangle\big)\Big],
\end{aligned} \quad (3.16)$$

where the P, $\widehat{P}$, Q and $\widehat{Q}$ represent the associated vector forms.

Proposition 3.2. The scheme (3.15) is unconditionally stable in the L^2 norm, i.e.

$$\|U^{n+1}\|^2+\|V^{n+1}\|^2=\|U^n\|^2+\|V^n\|^2.$$

Proof. By decomposing the scheme (3.15) into the real and imaginary parts and applying the similar procedures as the proof for the scheme (3.8), we obtain the unconditional stability for the scheme (3.15). □

4 Numerical experiments

In this section, we present various numerical experiments for the symplectic DSC schemes (3.9) and (3.15) with respect to the NLS equation (3.1) and CNLS equations (3.10). For the NLS equation, we give comprehensive numerical comparisons of the symplectic RSK and RDK with symplectic FDM, PSM, WCM, which can be easily derived by replacing the differential matrix D_2 with that of each method. For clarity, we list the first two derivatives for these methods as follows:

- Differential matrix for the FDM

$$\widehat{D}_1=\frac{1}{h}\begin{pmatrix}
-1 & 1 & & & \\
 & -1 & 1 & & \\
 & & \ddots & \ddots & \\
 & & & -1 & 1\\
1 & & & & -1
\end{pmatrix},\quad
\widehat{D}_2=\frac{1}{h^2}\begin{pmatrix}
-2 & 1 & & & 1\\
1 & -2 & 1 & & \\
 & \ddots & \ddots & \ddots & \\
 & & 1 & -2 & 1\\
1 & & & 1 & -2
\end{pmatrix}. \quad (4.1)$$

https://doi.org/10.4208/cicp.scpde14.32s Published online by Cambridge University Press

- Differential matrix for the PSM [27]

$$(\widetilde{D}_1)_{i,j}=\begin{cases}\frac{1}{2}\nu(-1)^{i+j}\cot\big(\nu(x_i-x_j)/2\big), & i\neq j,\\ 0, & i=j,\end{cases} \tag{4.2}$$

$$(\widetilde{D}_2)_{i,j}=\begin{cases}\frac{1}{2}\nu^2(-1)^{i+j+1}\csc^2\big(\nu(x_i-x_j)/2\big), & i\neq j,\\ -\nu^2\big(2(N/2)^2+1\big)/6, & i=j,\end{cases} \tag{4.3}$$

where $\nu=2\pi/(b-a)$. Note that the spectral differential matrix is full and for conventional solvers it needs large storages and computational costs. Fortunately we have the FFT algorithm and the computational costs will be reduced dramatically.

- Differential matrix for the WCM [11]

$$(\overline{D}_k)_{i,j}=\begin{cases}2^{kJ}\theta^{(k)}(i-j), & -W+1\leq j-i\leq W+1,\\ 2^{kJ}\theta^{(k)}(-s), & i-j=N-s,\ 1\leq s\leq W-1,\\ 2^{kJ}\theta^{(k)}(s), & j-i=N-s,\ 1\leq s\leq W-1,\\ 0, & \text{otherwise},\end{cases} \tag{4.4}$$

where W represents the order of a Daubechies scaling function $\phi(x)$ and we denote WCMW for the corresponding WCM method. Here, J is the level of resolution. $\theta(x)$ is the autocorrelation function of $\phi(x)$. The bandwidth of $\overline{D}_k$ is $2W-1$. There are no analytical expressions for the kth order derivatives $\theta^{(k)}(x)$. One can only obtain the values at dyadic points by recursive computation. Therefore, a subroutine is requested to compute this differential matrix, for example, the matrix method [28].

Besides the accuracy and efficiency tests, we also consider the invariant-preserving ability of different kinds of methods. For the continuous case of the NLS and CNLS equations with periodic boundary or zero boundary condition, the following global quantities are conserved which are named as charge, momentum and energy conservation laws respectively

$$I_1=\int_a^b|u|^2dx,\quad I_2=\mathrm{i}\int_a^b(u\bar{u}_x-\bar{u}u_x)dx,\quad I_3=\frac{1}{2}\int_a^b(\frac{1}{2}\varepsilon|u|^4-|u_x|^2)dx,$$

and

$$\widehat{I}_1=\int_a^b(|u|^2+|v|^2)dx,\quad \widehat{I}_2=\int_a^b(u\bar{u}_x+v\bar{v}_x)dx,$$
$$\widehat{I}_3=\frac{1}{2}\int_a^b\Big[\frac{1}{2}(|u|^4+|v|^4)-\kappa(|u_x|^2+|v_x|^2)+\beta|u|^2|v|^2\Big]dx.$$

https://doi.org/10.4208/cicp.scpde14.32s Published online by Cambridge University Press

The corresponding discrete forms of these invariants are taken as

$$I_1^n=\|U^n\|^2,\quad I_2^n=h(U^n)^TD_1\bar{U}^n-h(\bar{U}^n)^TD_1U^n,\quad I_3^n=\frac{1}{2}\Big(\frac{1}{2}\varepsilon\|U^n\|^4-\|D_1U^n\|^2\Big),$$

and

$$\begin{aligned}&\widehat{I}_1^n=\|U^n\|^2+\|V^n\|^2,\quad \widehat{I}_2^n=h(U^n)^TD_1\bar{U}+h(V^n)^TD_1\bar{V},\\&\widehat{I}_3^n=\frac{1}{2}\Big[\frac{1}{2}(\|U^n\|^4+\|V^n\|^4)-\kappa(\|D_1U^n\|^2+\|D_1V^n\|^2)+\beta\||U^n|\cdot|V^n|\|^2\Big].\end{aligned}$$

Errors in the L^∞-norm between the numerical solution u_j^n and the analytical solution $u(x_j,t_n)$, and errors in the above invariants are defined as

$$\begin{aligned}&e^n=\max_j|u_j^n-u(x_j,t_n)|,\\&E_i^n=I_i^n-I_i^0\quad \widehat{E}_i^n=\widehat{I}_i^n-\widehat{I}_i^0.\end{aligned}$$

We use the fixed-point iteration to solve the nonlinear systems (3.9) and (3.15) with tolerance 1E−14. The parameters in the DSC methods are chosen as $M=30$, $r=3.5$ and $L=71$ in all the following experiments except special requirement. We note that as long as the L value is chosen sufficiently large $L>M$, the numerical results are not sensitive to the specific values used.

Example 4.1. We show an accuracy test for the NLS equation (3.1) with $\varepsilon=2$ and the soliton solution

$$u(x,t)=\operatorname{sech}(x-4t)\exp\left(2\mathrm{i}\left(x-\frac{3}{2}t\right)\right).\tag{4.5}$$

All the symplectic schemes, i.e., the FDM, PSM, WCM30 and DSC including the RSK and RDK can simulate the soliton propagation well. We plot the waveforms in Fig. 2.

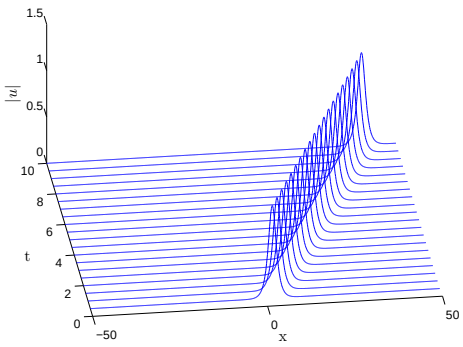


Figure 2: Soliton propagation by any of the symplectic schemes with $N=800$, $\tau=0.001$.

https://doi.org/10.4208/cicp.scpde14.32s Published online by Cambridge University Press

Table 1: Accuracy tests for different kinds of methods with $\tau=1\text{E}-6$ at $t=1$.

N	L^∞ error				
	FDM	PSM	WCM30	RSK	RDK
100	0.83	0.27	0.33	0.32	0.30
200	0.80	2.70E-3	4.97E-3	2.41E-3	2.41E-3
400	0.23	2.08E-8	1.70E-6	2.41E-7	2.34E-7
800	0.05	1.36E-11	3.55E-11	1.25E-11	1.24E-11

Table 2: Computational costs for different kinds of methods with $\tau=1\text{E}-6$ and $t=1$.

N	PSM	WCM30	RSK	RDK
100	93.82	94.42	94.40	94.88
200	131.34	130.45	130.36	130.11
400	206.70	208.87	206.51	207.40
800	381.96	382.97	385.02	385.31

The L^∞ errors for these schemes are listed in Table 1. The time step is fixed at $\tau=1\text{E}-6$ so that the errors are dominated by the spatial discretization. Apparently, the accuracy of the FDM method is only of order 2 while the other methods all decay at an exponential rate. More specifically, the two DSC methods with any N are more accurate than the WCM30 although the bandwidths of the associated differential matrices are nearly the same. The errors are also comparable to that of the PSM and when $N=200,800$, the results of RDK are even better. Among the two DSC method, RSK and RDK, the latter one is a little more accurate because it has one more parameter L to control the errors.

Next, we consider the invariant-preserving abilities of these symplectic schemes. Fig. 3 presents the errors in the three invariants for different methods respectively which shows that the PSM performs best among the four methods. As the theoretical proof, the charge invariant is preserved to round-off error by all the methods. Moreover, since the momentum is a quadratic invariant, with the high accurate approximations for the first order derivative by the PSM, WCM30, RSK and RDK, the momentum is also conserved exactly. For the energy invariant, although all the methods fail to preserve it precisely, the errors are bounded for a long time interval. We can hardly tell the difference in the errors of E_3 for the WCM30, RSK and RDK. From the zoom figure, the error of RDK is slightly smaller than the WCM30.

Example 4.2. In this example, we show the bound state solution [29] of the NLS equation (3.1) with the initial condition

$$u(x,0)=\text{sech}(x).$$

It will generate a bound state of $\widetilde{N}$ solitons if

$$\varepsilon=2\widetilde{N}^2.$$

https://doi.org/10.4208/cicp.scpde14.32s Published online by Cambridge University Press

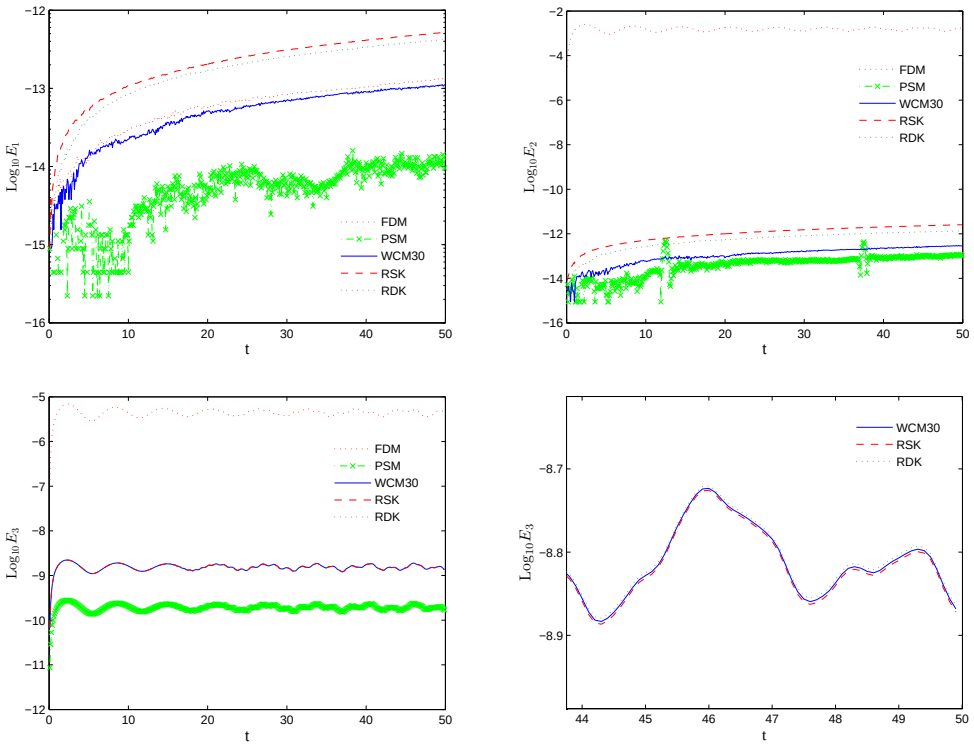


Figure 3: Errors in the invariants E_1, E_2 and E_3 for different methods with $N=800$, $\tau=0.001$. The right bottom figure amplifies the errors E_3 in the interval $[44,50]$.

The solutions develop small narrow structure which are difficult to resolve [30] if $\widetilde{N}\geq 3$. We take $\widetilde{N}=5$ for the RSK and RDK schemes in our test. Fig. 4 shows the time evolution of the solution as well as its contour plot in 15 time periods which can be both simulated by the two schemes. From the snapshots at four different times, we can see that the narrow structures are resolved very sharply. The corresponding errors in three invariants are presented in Fig. 5 which seems that the RSK and RDK produce the errors very closed to each other. More specifically, The charge invariant is preserved to round-off error and the errors in E_2 can be negligible. Due to the continual collision of the peaks, the energy invariant I_3 oscillates with rather small amplitudes.

Example 4.3 We consider the homoclinic structure of the NLS equation (3.1) with the following periodic initial condition [11]

$$u(x,0)=A\left(1+0.05\cos\left(\frac{\sqrt{2}}{4}x\right)\right),\quad x\in[-2\sqrt{2}\pi,2\sqrt{2}\pi],$$

which is in the vicinity of the homoclinic structure associated with the NLS equation and makes it difficult to simulate the solution. By varying the parameter A, we can change

https://doi.org/10.4208/cicp.scpde14.32s Published online by Cambridge University Press

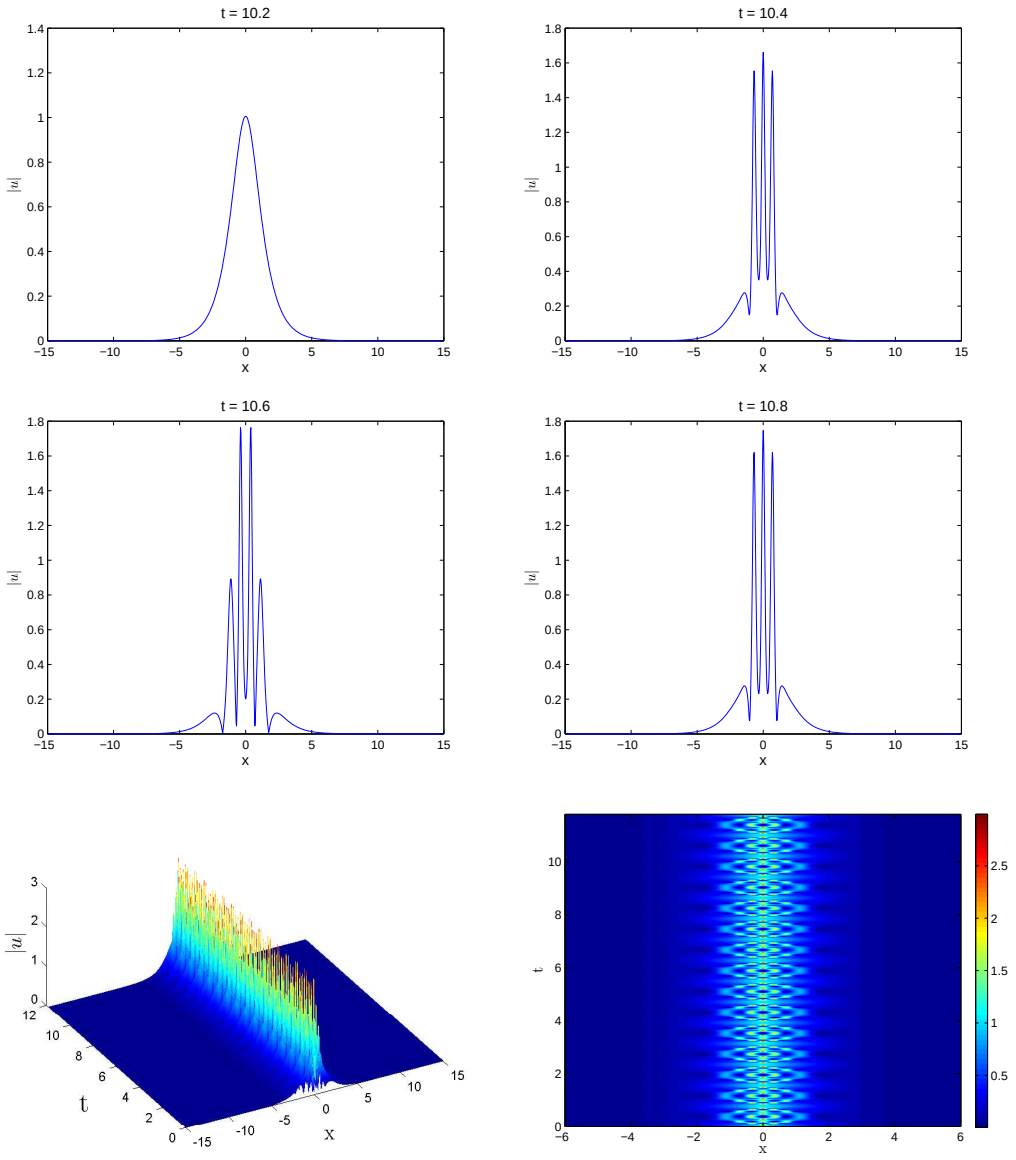


Figure 4: Wave propagations by the RSK or RDK and its contour plot with $N=1000$, $\tau=0.00002$.

the complexity of the homoclinic structure [12,31,32] which is a good robust test bed for our schemes. We first take $A=0.5$. Fig. 6 gives the wave propagation in the large interval $t\in[0,200]$ and its contour figure by the RSK or RDK which show that the two schemes can resolve the homoclinic structure very well. The related errors in invariants are presented in Fig. 7. As that of the above example, the two kinds of errors are nearly the same. Next, we increase A to $A=0.75$ and $A=1$. Consequently, the complexity of the homoclinic structure is increased. From Fig. 8, it is clear that the spatial symmetry is well preserved

https://doi.org/10.4208/cicp.scpde14.32s Published online by Cambridge University Press

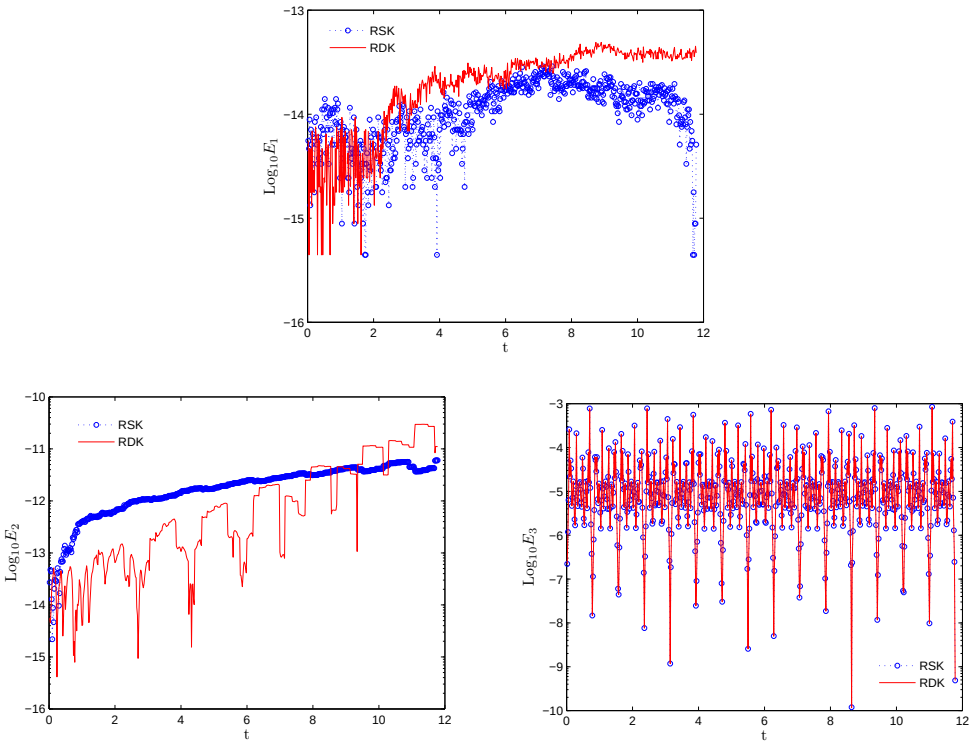


Figure 5: Errors in three invariants of the RSK and RDK with $N=1000$, $\tau=0.00002$.

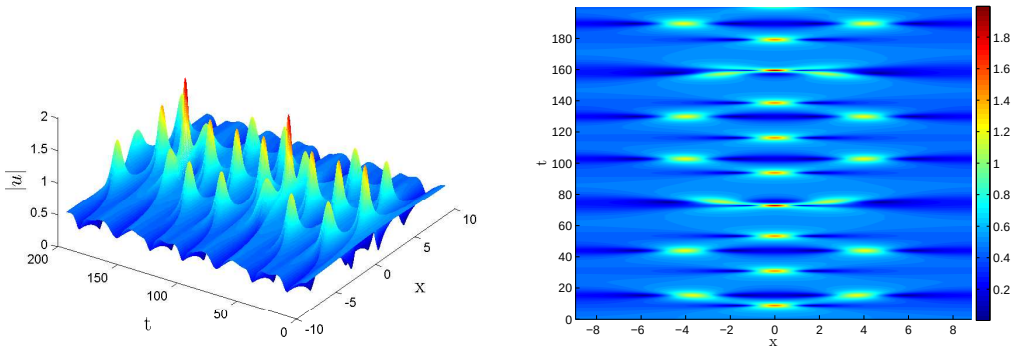


Figure 6: Wave propagation simulated by the RSK or RDK with $A=0.5$, $N=150$, $\tau=0.002$.

and no instability occurs for both two cases.

In the following examples, we test the symplectic RSK and RDK methods for the CNLS equations (3.10) with periodic boundary conditions. Since the numerical behaviours of the RSK and RDK are similar in accuracy, computational cost and invariant preservation, we only present the numerical results by the symplectic RSK scheme (3.15).

https://doi.org/10.4208/cicp.scpde14.32s Published online by Cambridge University Press

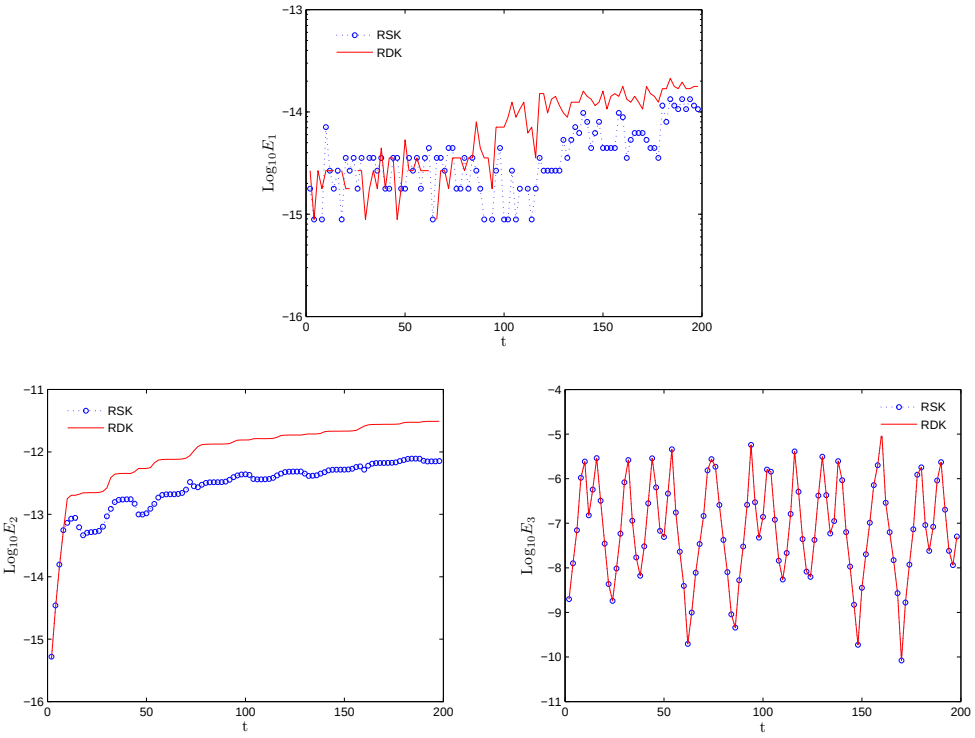


Figure 7: Errors in three invariants of the RSK and RDK with $N=150$, $\tau=0.002$.

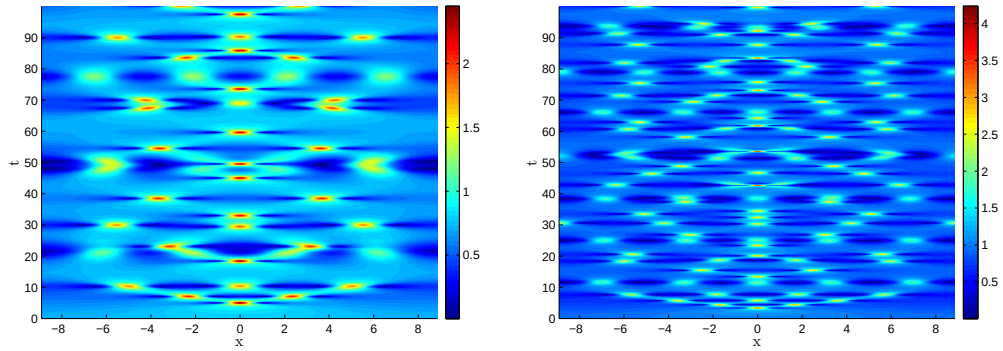


Figure 8: Wave propagation simulated by the RSK or RDK with $A=0.75$ (left), $A=1$ (right) and $N=300$, $\tau=0.0005$.

Example 4.4. Consider $\kappa=\frac{1}{2}$, then the CNLS equations (3.10) admit the solitary wave solution

$$u(x,t)=\sqrt{\frac{2\alpha}{1+\beta}}\mathrm{sech}\left(\sqrt{2\alpha}(x-vt)\right)\exp\left(\mathrm{i}\left(vx-\left(\frac{v^2}{2}-\alpha\right)\right)\right),$$

$$v(x,t)=-\sqrt{\frac{2\alpha}{1+\beta}}\mathrm{sech}\left(\sqrt{2\alpha}(x-vt)\right)\exp\left(\mathrm{i}\left(vx-\left(\frac{v^2}{2}-\alpha\right)\right)\right).$$

https://doi.org/10.4208/cicp.scpde14.32s Published online by Cambridge University Press

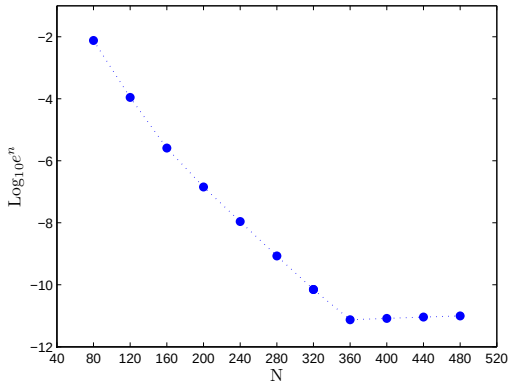


Figure 9: Errors between the numerical and analytical solutions with $\tau=1\mathrm{E}-6$ and different N.

We take the spatial interval $[-20,20]$ and the parameters $\alpha=1,\beta=\frac{2}{3},v=1$. Fig. 9 plots the error between the numerical and analytical solution of $u(x,t)$ at $t=1$. The errors are computed in L^2 norm w.r.t N and drawn on a semi-log scale so the slope of the error line indicates the expected exponential convergence rate.

$$u(x,0)=\sum_{i=1}^{2}\sqrt{\frac{2\alpha_i}{1+\beta}}\mathrm{sech}\big(\sqrt{2\alpha_i}(x-\xi_i)\big)\exp\big(\mathrm{i}v_i(x-\xi_i)\big),$$
$$v(x,0)=\sum_{i=1}^{2}\sqrt{\frac{2\alpha_i}{1+\beta}}\mathrm{sech}\big(\sqrt{2\alpha_i}(x-\xi_i)\big)\exp\big(\mathrm{i}v_i(x-\xi_i)\big),$$

where we set $\alpha_1=1$, $\alpha_2=0.5$, $\beta=1$, $v_1=-v_2=0.5$, $\xi_1=0$, $\xi_2=25$ and the computational domain $[-20,40]$. Fig. 10 presents the waveforms of $|u|$ in $t\in[0,50]$ and the related in-

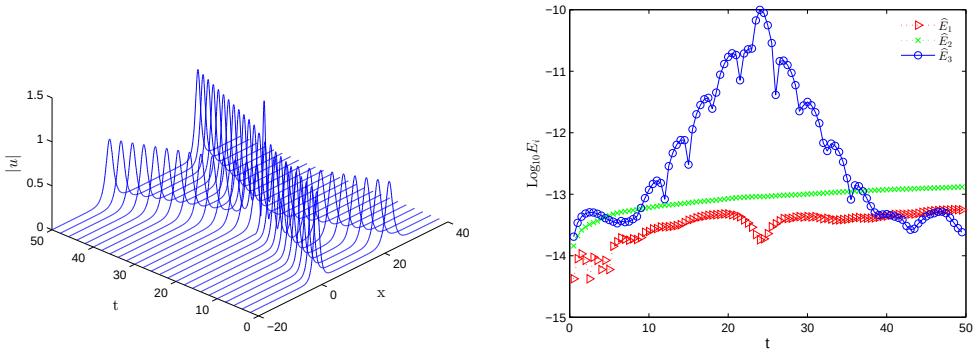


Figure 10: The numerical waveforms and the related errors in three invariants for two solitons collisions with $N=600$, $\tau=0.001$.

https://doi.org/10.4208/cicp.scpde14.32s Published online by Cambridge University Press

variants errors. We can see clearly that the collision of the two solitons is elastic and the speeds and directions remain the same after collision. The three invariants are also conserved very well. The errors in E_3 increase when the collision takes place and then return to a smaller amplitude.

We know from [33, 34] that when $\beta=0$ and $\beta=1$, the CNLS system (3.10) is an integrable system and the collision of the solitary waves is elastic. Otherwise, there will occur various collision scenarios such as transmission, reflection, fusion, creation of solitary waves [35, 36]. In the following tests, we take the initial condition as

$$u(x,0)=\sqrt{2}r_1\mathrm{sech}(r_1x+\xi_1)\exp(\mathrm{i}v_1x),$$
$$v(x,0)=\sqrt{2}r_2\mathrm{sech}(r_2x+\xi_2)\exp(\mathrm{i}v_2x),$$

where the parameters are fixed to $\kappa=1$, $r_1=1.2$, $r_2=1$, $\xi_1=10$, $\xi_2=-10$. The grid numbers are $N=400$ and the time step is $\tau=0.005$. By varying the values of β and the velocity $v_1=-v_2=V/4$, we can simulate the above mentioned scenarios by the scheme RSK.

Example 4.5. We first set $\beta=2/3$ and the approaching velocity $V=0.4$. By this choice, we can observe the reflection scenario in Fig. 11. During collision, the velocity of the right-moving soliton steadily decreases, and becomes negative when it emerges from the collision. This means that this soliton is reflected back by collision. The same thing happens to the soliton $|v|$. It initially moves to the left, but turns around after collision. Then we increase the velocity to $V=1.6$ and check the transmission scenario. We can see from Fig. 12 that the velocities decrease significantly as before. But in this case, they pick up speed again when they emerge from the collision. As a result, the solitons pass through each other, and settle down to constant speeds along the original directions. It should be noticed that the charge and momentum are preserved to round-off error for both two cases. While for the energy invariant, the error magnitudes increase after the collision but are bounded during the whole computation interval.

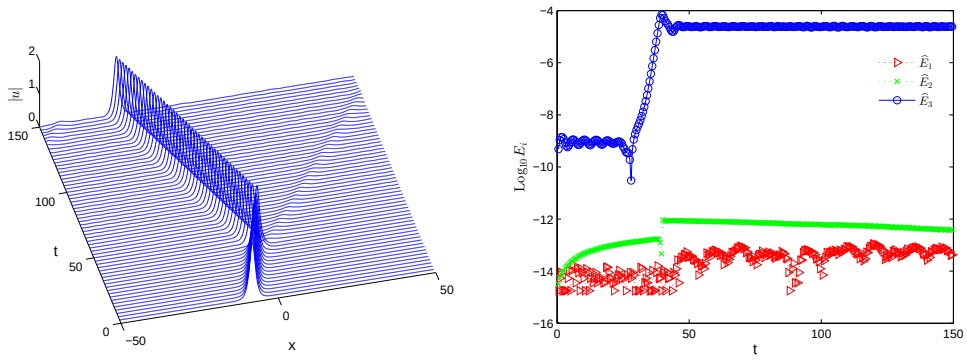


Figure 11: Reflection scenario and errors in the invariants with $\beta=2/3$, $V=0.4$.

https://doi.org/10.4208/cicp.scpde14.32s Published online by Cambridge University Press

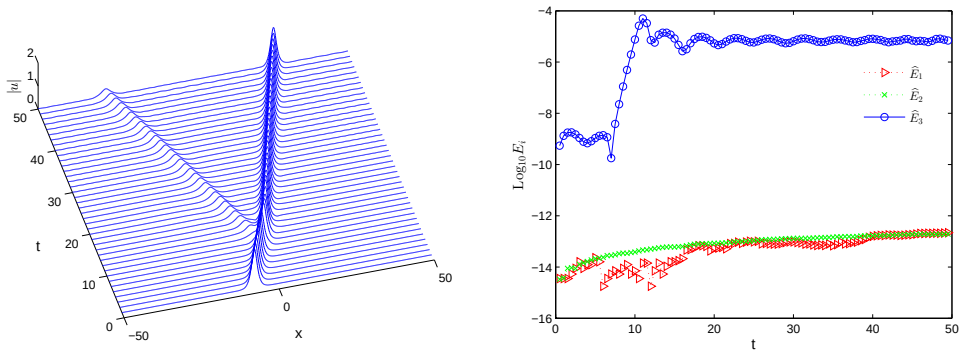


Figure 12: Transmission scenario and errors in the invariants with $\beta=2/3$, $V=1.6$.

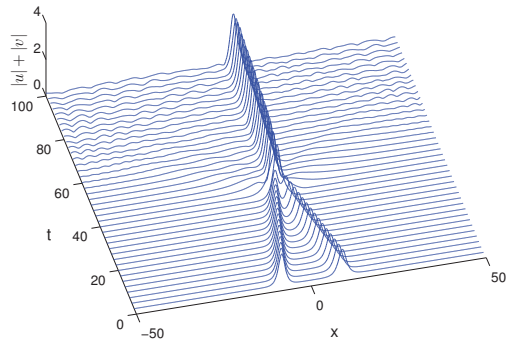


Figure 13: Fusion of two solitons: $|u|+|v|$ with $\beta=0.3$, $V=0.4$.

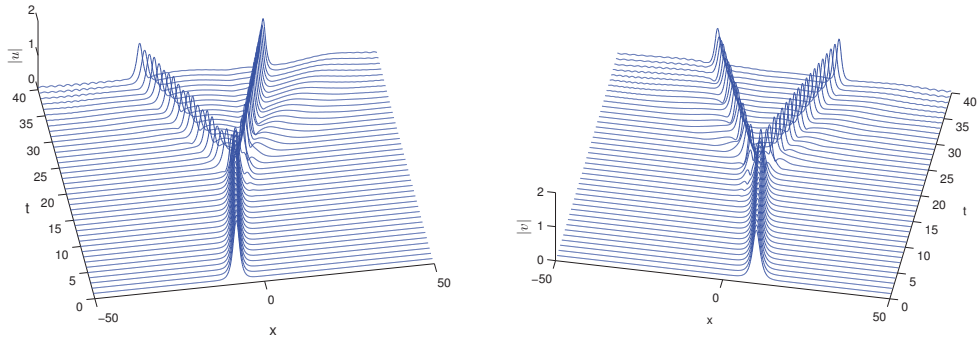


Figure 14: Creation scenario: $|u|$, $|v|$ with $\beta=2$, $V=0.8$.

In the last two examples, we simulate the fusion scenario and the creation of new soliton. We first set $\beta=0.3$, $V=0.4$. Fig. 13 presents the wave propagation of the two solitons. We can see that from Fig. 13 the two solitons fusion into one soliton after the collision. Next, we fix $\beta=2$, $V=0.8$, as demonstrated in Fig. 14, a new soliton has been

https://doi.org/10.4208/cicp.scpde14.32s Published online by Cambridge University Press

created. To sum up, the scheme RKS simulates the interaction of the two solitons clearly for different β and V. Moreover, the three invariants are preserved precisely as expected.

5 Concluding remarks

This paper introduces a new candidate of differential matrices for constructing symplectic schemes by the discrete singular convolution method. We derive the analytical expressions for two kinds of differential matrices with respect to the regularized Shannon's kernel and Dirichlet kernel which belongs to the delta type kernel. Furthermore, the differential matrices are bandlimited and circulant such that FFT algorithms can be implemented for the periodic cases to reduce the computational cost remarkably. The computational accuracy is found to be competitive, or even better than the Fourier pseudospectral method. Based on this kind of differential matrices, we construct two novel symplectic schemes for the nonlinear Schrödinger equation and the coupled Schrödinger equations, respectively. Comprehensive numerical experiments are presented including comparisons with the finite difference method, the Fourier pseudospectral method and the wavelet collocation method.

Note that this kind of differential matrices can be applied on the general Hamiltonian PDEs, such as the KdV equation, the Maxwell's equations, the Camassa-Holm equation and so on. Furthermore, besides the symplectic schemes, one can also use the differential matrices to construct other structure-preserving methods, like the multisymplectic schemes [37], the energy and momentum preserving schemes [38] and so on.

Acknowledgments

This research work is supported by National Natural Science Foundation of China (under Grant Nos. 41274103, 11271195, 41504078), National Basic Research Program of China (2014CB845906), National R&D Projects for Key Scientific Instruments (ZDYZ2012-1-02-04), and KZZD-EW-TZ-15-3 program from Chinese Academy of Sciences, China Postdoctoral Science Foundation funded project (119103S257).

References

[1] K. Feng and M.Z. Qin. The symplectic methods for the computation of Hamiltonian equations. In You-Ian Zhu and Ben-yu Guo, editors, *Numerical Methods for Partial Differential Equations*, volume 1297 of *Lecture Notes in Mathematics*, pages 1–37. Springer Berlin Heidelberg, 1987.

[2] J.M. Sanz-Serna and M.P. Calvo. *Numerical Hamiltonian problems*. Chapman & Hall, 1994.

[3] E. Hairer, C. Lubich, and G. Wanner. *Geometric Numerical Integration: Structure-Preserving Algorithms for Ordinary Differential Equations*. Springer, Berlin, 2002.

[4] R.I McLachlan and G.R.W. Quispel. Geometric integrators for ODEs. *J. Phys. A: Math. Gen.*, 39:5251, 2006.

https://doi.org/10.4208/cicp.scpde14.32s Published online by Cambridge University Press

[5] U.M. Ascher and R.I. Mclachlan. On symplectic and multisymplectic schemes for the KdV equation. *J. Sci. Comput.*, 25:83–104, 2005.
[6] Y.S. Wang, B. Wang, Z.Z. Ji, and M.Z. Qin. High order symplectic schemes for the sine-Gordon equation. *J. Phys. Soc. Jpn.*, 72:2731–2736, 2003.
[7] D.L. Wang. Semi-discrete Fourier spectral approximations of infinite dimensional Hamiltonian system and conservation laws. *Comput. Math. Appl.*, 21:63–75, 1991.
[8] J.B. Chen. Symplectic and multisymplectic Fourier pseudospectral discretizations for the Klein-Gordon equation. *Lett. Math. Phys.*, 75:293–305, 2006.
[9] J.W. Ma and H.Z. Yang. Multiresolution symplectic scheme for wave propagation in complex media. *Appl. Math. Mech.*, 25:573–579, 2004.
[10] J.W. Ma. An exploration of multiresolution symplectic scheme for wave propagation using second-generation wavelets. *Phys. Lett. A*, 328:36–46, 2004.
[11] H.J. Zhu, L.Y. Tang, S.H. Song, Y.F. Tang, and D.S. Wang. Symplectic wavelet collocation method for Hamiltonian wave equations. *J. Comput. Phys.*, 229:2550–2572, 2010.
[12] R.I. McLachlan. Symplectic integration of Hamiltonian wave equations. *Numer. Math.*, 66:465–492, 1994.
[13] A.L. Islas, D.A. Karpeev, and C.M. Schober. Geometric integrators for the nonlinear Schrödinger equation. *J. Comput. Phys.*, 173:116–148, 2001.
[14] L.H. Kong, J.L. Hong, L. Wang, and F.F. Fu. Symplectic integrator for nonlinear high order Schrödinger equation with a trapped term. *J. Comput. Appl. Math.*, 231:664–679, 2009.
[15] Y.J. Sun and P.S.P. Tse. Symplectic and multisymplectic numerical methods for Maxwell's equations. *J. Comput. Phys.*, 230:2076–2094, 2011.
[16] W. Sha, Z.X. Huang, M.S. Chen, and X.L. Wu. Survey on symplectic finite-difference time-domain schemes for Maxwell's equations. *IEEE Trans. Antennas Propag.*, 56:493–500, 2008.
[17] L.H. Kong, J.L. Hong, F.F. Fu, and J.Chen. Symplectic structure-preserving integrators for the two-dimensional Gross-Pitaevskii equation for BEC. *J. Comput. Appl. Math.*, 235:4937–4948, 2011.
[18] Y.M. Tian and M.Z. Qin. Explicit symplectic schemes for investigating the evolution of vortices in a rotating Bose-Einstein Condensate. *Comput. Phys. Commun.*, 155:132–143, 2003.
[19] G.W. Wei. Discrete singular convolution for the solution of the Fokker-Planck equation. *J. Chem. Phys.*, 110:8930–8942, 1999.
[20] G.W. Wei. A unified approach for solving the Fokker-Planck equations. *J. Phys. A*, 33:4935–4953, 2000.
[21] S. Zhao and G.W. Wei. Comparison of the discrete singular convolution and three other numerical schemes for solving Fisher's equation. *SIAM J. Sci. Comput.*, 25:127–147, 2003.
[22] S.Y. Yang, Y.C. Zhou, and G.W. Wei. Comparison of the discrete singular convolution algorithm and Fourier pseudospectral method for solving partial differential equations. *Comput. Phys. Commun.*, 143:113–135, 2002.
[23] G.W. Wei. Discrete singular convolution method for the sine-Gordon equation. *Physica D*, 137:247–259, 2000.
[24] B.F. Feng and G.W. Wei. A comparison of the spectral and the discrete singular convolution schemes for the KdV type equations. *J. Comput. Appl. Math.*, 145:183–188, 2002.
[25] X.F. Li, W.S. Wang, M.W. Lu, M.G. Zhang, and Y.Q. Li. Structure-preserving modelling of elastic waves: a symplectic discrete singular convolution differentiator method. *Geophys. J. Int.*, 188:1382–1392, 2012.
[26] S. Zhao and G.W. Wei. A unified discontinuous Galerkin framework for time integration. *Math. Method Appl. Sci.*, 37:1042–1071, 2014.

https://doi.org/10.4208/cicp.scpde14.32s Published online by Cambridge University Press

[27] J.B. Chen and M.Z. Qin. Multi-symplectic Fourier pseudospectral method for the nonlinear Schrödinger equation. *Electron. Trans. Numer. Anal.*, 12:193–204, 2001.
[28] I. Daubechies. *Ten Lectures on Wavelets*. SIAM, 1992.
[29] Y. Xu and C.-W. Shu. Local discontinuous Galerkin methods for nonlinear Schrödinger equations. *J. Comput. Phys.*, 205:72–97, 2005.
[30] J.W. Miles. An envelope soliton problem. *SIAM J. Appl. Math.*, 41:227–230, 1981.
[31] B.M. Herbst, F. Varadi, and M.J. Ablowitz. Symplectic methods for the nonlinear Schrödinger equation. *Math. Comput. Simul.*, 37:353–369, 1994.
[32] C.M. Schober. Symplectic integrators for the Ablowitz-Ladik discrete nonlinear Schrödinger equation. *Phys. Lett. A*, 259:140–151, 1999.
[33] M.J. Ablowitz and H. Segur. *Solitions and the Inverse Scattering Transform*. SIAM, Philadelphia, 1981.
[34] R.I. McLachlan. Multisoliton perturbation theory for the Manakov equations and its applications to nonlinear optics. *Phys. Rev. E*, 59:2393–2405, 1999.
[35] J.Q. Sun and M.Z. Qin. Multi-symplectic methods for the coupled 1D nonlinear Schrödinger system. *Comput. Phys. Commun.*, 155:221–235, 2003.
[36] Y.S. Wang and S.T. Li. New schemes for the coupled nonlinear Schrödinger equation. *Int. J. Comput. Math.*, 87:775–787, 2008.
[37] T.J. Bridges and S. Reich. Multi-symplectic integrators: numerical schemes for Hamiltonian PDEs that conserve symplecticity. *J. Comput. Phys.*, 157:473–499, 2000.
[38] Y.Z. Gong, J.X. Cai, and Y.S. Wang. Some new structure-preserving algorithms for general multi-symplectic formulations of Hamiltonian PDEs. *J. Comput. Phys.*, 279:80–102, 2014.

https://doi.org/10.4208/cicp.scpde14.32s Published online by Cambridge University Press